Phase-shift error in quadrature-detection-based interferometers

Peter Gregorčič*, Tomaž Požar, Janez Možina
Faculty of Mechanical Engineering, University of Ljubljana, Aškerčeva 6, 1000 Ljubljana, Slovenia

ABSTRACT

This contribution investigates the influence of phase shift on the measured displacement error in interferometers based on quadrature detection. This error was experimentally investigated using a two-detector homodyne quadrature laser interferometer (HQLI) with two orthogonally polarized signals. Here, the phase shift can be continuously varied by rotating a wave plate. However, the rotation of the wave plate also produces unequal signal amplitudes and different zero offsets, both of which can be corrected with an appropriate signal processing. The measured phase-shift error perfectly agrees with the theoretically determined phase-shift error region. This error is systematic, periodic and severely asymmetrical around the nominal displacement value. For the robust realization of a HQLI, a slight deviation from the aligned angle of the wave plate should not shift the phase significantly from the ideal 90°. This may pose a problem if an additional phase shift originates from the polarization-sensitive light reflections, such as the reflection at the non-polarizing beam splitter.

Keywords: homodyne quadrature laser interferometer, metrology, nonlinearity, phase-shift error

1. INTRODUCTION

Many interesting applications, such as: measurements of high-amplitude ultrasound on stationary and moving objects[2] and metrology analysis including scanning probe microscopes[1] call for a contactless, sub-fringe resolution, and high-dynamic-range displacement-measuring method with a constant sensitivity. The precision and accuracy of interferometric methods based on two or more signals in phase quadrature, which satisfy all of the above requirements, are limited by a set of errors[3,4] that generally arise from mechanical, optical, and electric sources.

Homodyne quadrature-detection-based interferometers allow measurements of displacements that are several orders of magnitude longer than the interferometric wavelength λ with a typical resolution of 10^{-3} λ. Their attainable accuracy is limited by four major factors: the uncertainty of the laser's wavelength in vacuum; the uncertainty of the refractive index through which the laser beam propagates[5]; the ability to count the interference fringes bidirectionally; and lastly, the resolution of sub-fringe detection. The first three factors limit the attainable measurement range while the last one defines the minimal resolvable distance. This distance is fundamentally limited by a theoretical lowest attainable signal-to-noise ratio of the photodetector, but practically, it is mainly restrained by the three commonly encountered systematic nonlinearities: unequal AC amplitudes, DC offsets, and quadrature phase-shift error.

When the phase shift between the detected signals deviates from the ideal 90°, the phase-unwrapping procedure generates an error in the displacement. To analyze this error experimentally, other errors (e.g., unequal gains, zero offsets, deviations from the harmonic signal shape, etc.) need to be eliminated or corrected. This can be most conveniently realized in a homodyne quadrature laser interferometer (HQLI) with two orthogonally polarized signals. In a HQLI, the phase shift can be continuously varied by rotating a wave plate. However, the rotation of the wave plate also produces unequal signal amplitudes and different zero offsets, both of which can be corrected with the appropriate signal processing, presented in Ref. 3. Even though the lack of quadrature can be determined and corrected, it always ruins the constant sensitivity due to which the resolution of the interferometer varies periodically. Moreover, an inappropriate phase shift also results in an unwanted reduction of the visibilities in both channels.

With an appropriate alignment of the optical components in the homodyne quadrature interferometer the nonlinearities can be significantly reduced[6]. However, for the robust realization any slight deviation of the optical components from the aligned position should not significantly alter the nonlinearities. This may pose a problem if an additional phase shift originates from the polarization-sensitive light reflections, such as the reflection at the non-polarizing beam splitter.

*peter.gregorcic@fs.uni-lj.si; phone +386 1 4771 172

Optical Sensing and Detection, edited by Francis Berghmans, Anna Grazia Mignani, Chris A. van Hoof,
Proc. of SPIE Vol. 7726, 77260X · © 2010 SPIE · CCC code: 0277-786X/10/$18 · doi: 10.1117/12.854759

This paper investigates the error due to the lack of quadrature with a two-detector homodyne laser interferometer. This error is systematic, periodic and severely asymmetrical around the nominal displacement value. The main results presented in this paper can also be used to assess and correct the detector errors of other interferometric and non-interferometric displacement-measuring devices based on phase-quadrature detection.

2. EXPERIMENTAL SETUP

There are two basic variants of the HQLI with regard to the number of detected signals. A balanced scheme with four detectors uses all the available laser light, has twice the number of detectors, compared to the two-detector variant, and more than twice the number of optical components[7]. However, several errors in the detected displacement may arise from misaligned or imperfect optical components[8]. With this in mind we realized an experimental two-detector HQLI, trying to reduce the possible errors (e.g., polarization-mixing cross talk[8]) that originate from the imperfect optical components. Since a detailed description of the HQLI can be found in Ref. 3, we will restrict ourselves here to a brief overview.

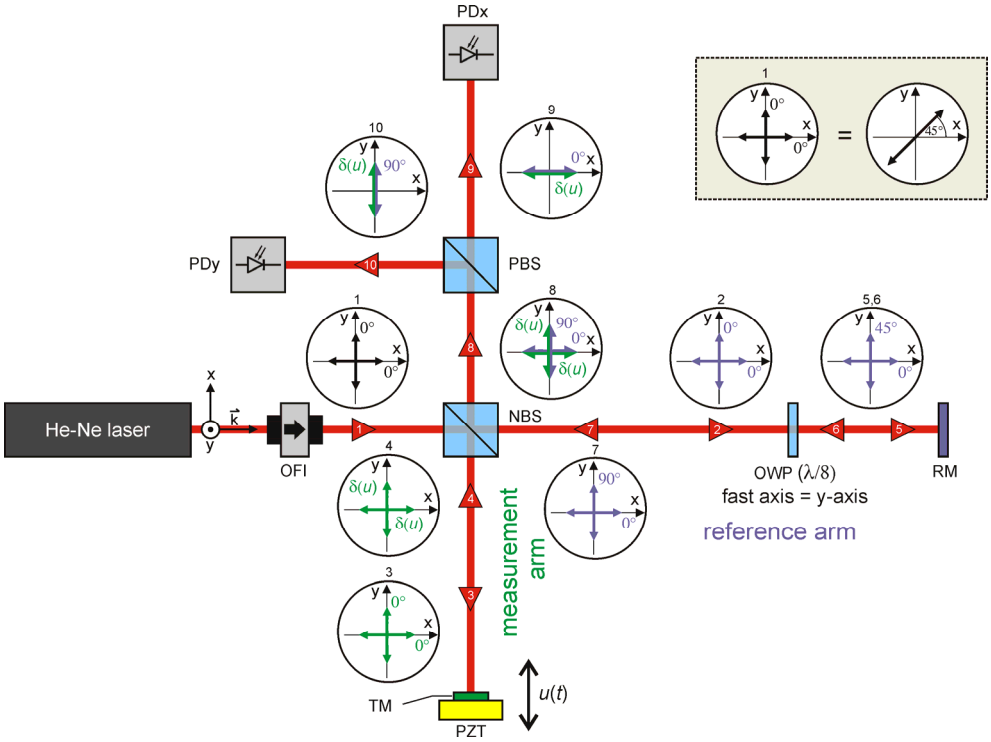

Figure 1. Schematic top view of the HQLI. The polarization states at the locations designated by the numbered arrows are indicated in the nearby circles. The exiting light from the He-Ne laser is linearly polarized in the *x*-plane. Optical components used in the HQLI are: optical Faraday isolator (OFI), non-polarizing beam splitter (NBS), octadic-wave plate (OWP), reference mirror (RM), target mirror (TM) mounted on the piezoelectric transducer (PZT), and polarizing beam splitter (PBS). Two signals are detected with photodiodes (PDy and PDx).

The top view of the HQLI setup is schematically illustrated in Fig. 1. The cylindrical head of the polarized and stabilized He-Ne laser (λ = 632.8 nm) is rotated so that the linearly polarized beam exiting the laser lies in the plane of the optical table (*x*-plane). After the optical Faraday isolator (OFI, arrow 1) the beam polarization forms a 45° angle with respect to the *x*-plane. As shown in the polarization scheme 1, this polarization can be decomposed into two orthogonal polarizations with equal intensities, one in the plane of the paper (*x*-axis) and the other perpendicular to it (*y*-axis). The 50%-50% non-polarizing beam splitter (NBS) evenly splits the beam into the reference (arrow 2) and measurement (arrow 3) arms. The first transition through the octadic-wave plate (OWP, arrow 5), which is placed in the reference arm, gives rise to the 45° (λ/8) phase difference between the orthogonal polarizations. The beam is then reflected from a reference mirror (RM) (arrow 6) and another 45° are added on the returning passage through the OWP (arrow 7). The orthogonal polarizations in the measurement arm experience an equal phase shift due to the movement of the target

mirror (TM) (arrow 4), which is driven by a piezoelectric transducer (PZT). The polarization states of the recombined beams (arrow 8) arriving from both arms are shown in polarization scheme 8. The light in phase opposition is not detected since it returns towards the laser and is blocked by the OFI. The polarizing beam splitter (PBS) transmits the *x*-polarization (arrow 9) and reflects the *y*-polarization (arrow 10).

Two interfering beams with polarizations in the *x*-plane, one from the reference arm and the other from the measurement arm, reach the photodiode PDx. Similarly, the perpendicular polarizations coming from both arms illuminate the photodiode PDy. Ideally, the interference signals on the photodiodes are shifted by 90°, which can be achieved with a properly rotated OWP. The measured displacement u is encoded in the phase $\delta(u) = 4\pi u/\lambda$, where λ is the wavelength of the interferometric laser.

3. THEORY

The operation of the two-detector HQLI with ideal optical components can be most conveniently described by the Jones matrix formalism on the propagation of plane light waves. This theoretical analysis was already done by the authors in the previous paper[3], therefore only the main results will be presented here.

The intensities I_x and I_y reaching the photodiodes PDx and PDy depend on the optical phase δ and on the angle of the OWP rotation φ:

$$\begin{aligned} I_x(\delta,\varphi) &= \frac{I_0}{16}\left(4+\sin 4\varphi + 2\sqrt{2}\left(\cos\delta - \sin\delta\left(\cos 2\varphi + \sin 2\varphi\right)\right)\right), \\ I_y(\delta,\varphi) &= \frac{I_0}{16}\left(4-\sin 4\varphi + 2\sqrt{2}\left(\cos\delta + \sin\delta\left(\cos 2\varphi - \sin 2\varphi\right)\right)\right). \end{aligned} \tag{1}$$

Here, I_0 stands for the output intensity of the interferometric laser. Assuming a linear response of the photodiodes, the same dependence as in Eqs. (1) is expected in the measured amplified output voltages V_x and V_y from the photodiodes. Under ideal conditions, when the fast axis of the OWP is perpendicular to the *x*-plane, the signals are in phase quadrature:

$$I_x(\delta - 45°, 0°) = \frac{I_0}{4}\left(1+\cos\delta\right) \quad \text{and} \quad I_y(\delta - 45°, 0°) = \frac{I_0}{4}\left(1+\sin\delta\right). \tag{2}$$

A constant optical phase of 45° was subtracted from the varying optical phase δ in order to show that the signals on PDx and PDy vary as a cosine and sine functions, respectively. Thus, the signals are in a quadrature, i.e., 90° out of the phase.

The time dependent displacement $u(t)$ of the target mirror (TM) along the line of the laser beam is encoded in the optical phase as $\delta(u(t)) = 4\pi u(t)/\lambda$ and can be derived from the ideal quadrature signals I_x and I_y (Eqs. (2)) by subtracting the DC offset $I_0/4$ as:

$$u(t) = \frac{\lambda}{4\pi}\left(\arctan\frac{I_y - I_0/4}{I_x - I_0/4} + m\pi\right), \quad m = 0, \pm 1, \pm 2, \ldots. \tag{3}$$

The integer m has to be chosen correctly, so that the function $u(t)$ satisfies the condition of being continuous.

The rotation of the OWP has an influence on the phase shift between I_x and I_y, and their maximum and minimum values. To calculate these values, we need to find the extremes of Eqs. (1) with respect to δ for an arbitrary angle φ. The locations of the maxima are labeled $\delta_{Ix,Iy}^{\max}$, while the minima are labeled $\delta_{Ix,Iy}^{\min}$:

$$\begin{aligned} \delta_{Ix}^{\max}(\varphi) &= -\arctan\left(\sin 2\varphi + \cos 2\varphi\right), \\ \delta_{Iy}^{\max}(\varphi) &= -\arctan\left(\sin 2\varphi - \cos 2\varphi\right), \\ \delta_{Ix}^{\min}(\varphi) &= \pi - \arctan\left(\sin 2\varphi + \cos 2\varphi\right), \\ \delta_{Iy}^{\min}(\varphi) &= \pi - \arctan\left(\sin 2\varphi - \cos 2\varphi\right). \end{aligned} \tag{4}$$

Substituting the locations of the extremes (Eqs. (4)) back into Eqs. (1) gives the maximum and minimum values of the theoretically detectable intensities for an arbitrary angle φ:

$$
\begin{aligned}
I_x^{\max}(\varphi) &= I_x(\delta_{Ix}^{\max}(\varphi),\varphi) = \frac{I_0}{16}\left(4+\sin 4\varphi+2\sqrt{2}\sqrt{2+\sin 4\varphi}\right), \\
I_y^{\max}(\varphi) &= I_y(\delta_{Iy}^{\max}(\varphi),\varphi) = \frac{I_0}{16}\left(4-\sin 4\varphi+2\sqrt{2}\sqrt{2-\sin 4\varphi}\right), \\
I_x^{\min}(\varphi) &= I_x(\delta_{Ix}^{\min}(\varphi),\varphi) = \frac{I_0}{16}\left(4+\sin 4\varphi-2\sqrt{2}\sqrt{2+\sin 4\varphi}\right), \\
I_y^{\min}(\varphi) &= I_y(\delta_{Iy}^{\min}(\varphi),\varphi) = \frac{I_0}{16}\left(4-\sin 4\varphi-2\sqrt{2}\sqrt{2-\sin 4\varphi}\right).
\end{aligned}
\tag{5}
$$

Theoretical signals, when the OWP is rotated for an angle $\varphi = 60°$ with respect to the ideal angle, can be seen in the screenshot of Vid. 1. In this case, the amplitudes and the offsets of both signals are not the same, due to the lack of quadrature. During the full revolution of the OWP, the maximum values of the intensities $I_{x,y}$ vary in the interval between values $I_{x,y}/I_0 = (3+2\sqrt{2})/16 \approx 0.364$ and $I_{x,y}/I_0 = (5+2\sqrt{6})/16 \approx 0.619$, which is shown as a pale-gray-shaded region in Vid. 1. Similarly, the minimum values of the intensities $I_{x,y}$ vary between $I_{x,y}/I_0 = 0$ and $I_{x,y}/I_0 = (3-2\sqrt{2})/16 \approx 0.011$. This interval is marked with the dark-gray-shaded region in Vid. 1.

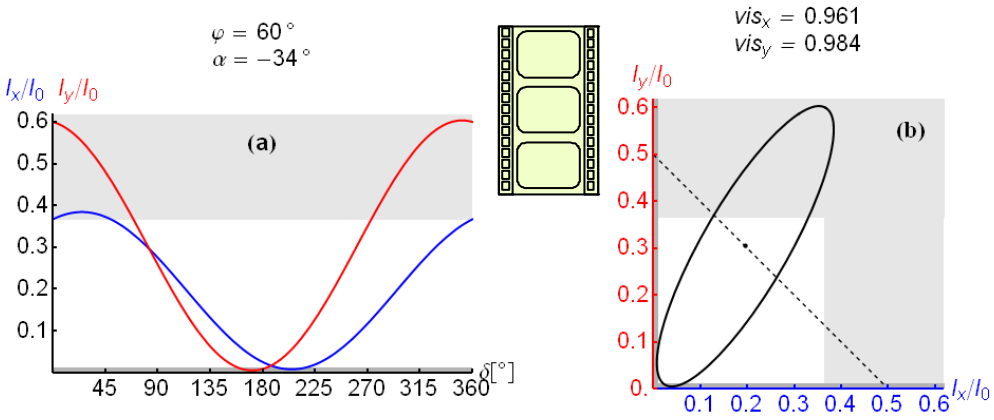

Video 1. Screenshot: (a) One period of the theoretical signals $I_{x,y}(\delta - 45°,60°)$ as a function of the optical phase δ. (b) Lissajous figure of the signals. Video: One period of the theoretical signals $I_{x,y}(\delta - 45°,\varphi)$ as a function of the optical phase δ for a continuously varying OWP angle φ from 0° to 180°. http://dx.doi.org/10.1117/12.854759.1

The relation between the phase shift α and the angle of the OWP rotation φ is defined as the difference between $\delta_{Iy}^{\max,\min}$ and $\delta_{Ix}^{\max,\min}$ as:

$$
\alpha(\varphi) = \delta_{Iy}^{\max,\min}(\varphi) - \delta_{Ix}^{\max,\min}(\varphi) = \arctan\left(\cos 2\varphi - \sin 2\varphi\right) - \arctan\left(\cos 2\varphi + \sin 2\varphi\right), \tag{6}
$$

while the sensitivity of the phase shift on the OWP rotation corresponds to the slope $d\alpha/d\varphi$, which can be extracted from Eq. (6) as:

$$
\frac{d\alpha(\varphi)}{d\varphi} = -\frac{4\left(5\sin 2\varphi + \sin 6\varphi\right)}{7+\cos 8\varphi}. \tag{7}
$$

The visibility is a standard figure of merit of an interferometer and is defined as:

$$vis_x(\varphi) = \frac{I_x^{\max}(\varphi) - I_x^{\min}(\varphi)}{I_x^{\max}(\varphi) + I_x^{\min}(\varphi)} = \frac{2\sqrt{2}\sqrt{2+\sin 4\varphi}}{4+\sin 4\varphi} \ ,$$
$$vis_y(\varphi) = \frac{I_y^{\max}(\varphi) - I_y^{\min}(\varphi)}{I_y^{\max}(\varphi) + I_y^{\min}(\varphi)} = \frac{2\sqrt{2}\sqrt{2-\sin 4\varphi}}{4-\sin 4\varphi} \ . \quad (8)$$

Here, $vis_{x,y}$ stands for the visibilities of both signals. The value $I_{x,y}^{\min}(\varphi)$ is in general not zero, since the destructive interference of the beams coming from both interferometric arms is even theoretically not perfect. The calculated visibilities for both signals are shown in Vid. 1(b). They reach the lowest value of $2\sqrt{2}/3 \approx 0.943$ and have one local minimum of $2\sqrt{6}/5 \approx 0.980$ per period.

The Lissajous figure of the signals, shown in Vid. 1(b), is obtained by plotting the vector $(I_x(\delta,\varphi),I_y(\delta,\varphi))$ for a fixed value of φ over a full period in δ. When the OWP is rotated, i.e., the phase shift varies, the center of the Lissajous figure $C(c_x,c_y)$ moves on the line, which connects the points $(0,I_0/2)$ and $(I_0/2,0)$ (the dashed line in Vid. 1(b)). The dependence of the coordinates c_x and c_y on the angle of OWP rotation is defined by:

$$c_x(\varphi) = \frac{I_x^{\max}(\varphi) + I_x^{\min}(\varphi)}{2} = \frac{I_0}{16}\left(4+\sin 4\varphi\right) \ ,$$
$$c_y(\varphi) = \frac{I_y^{\max}(\varphi) + I_y^{\min}(\varphi)}{2} = \frac{I_0}{16}\left(4-\sin 4\varphi\right) \ , \quad (9)$$

and are related with the equation $c_y = I_0/2 - c_x$.

The theoretical curves and values in Vid. 1 were obtained using Eqs. (1),(6),(8) and (9). The bordering lines of the two regions between the highest and lowest intensities (shown in Vid. 1), reached by the maximum and minimum value of $I_{x,y}$, were calculated by finding the extremes of Eqs. (5) with respect to φ. It should be noted that as the OWP is rotated, the signals $I_{x,y}$ experience an unequal change in AC amplitude and unequal DC offsets.

Assuming that the only significant nonlinearities of the measured voltage signals $V_{x,y}$ originate from the unequal AC amplitudes, two differing DC offsets, and the phase shift, we can easily normalize the voltage signals and subtract their DC shifts to obtain a pair of signals in the following form:

$$s_{xe} = \cos\delta \quad \text{and} \quad s_{ye} = \cos(\delta - \alpha) \ . \quad (10)$$

Here, the only remaining nonlinearity is due to phase shift. With $\alpha = 90°$ we obtain the ideal signals:

$$s_x = \cos\delta \quad \text{and} \quad s_y = \sin\delta \ . \quad (11)$$

The error in displacement caused by the lack of quadrature (dubbed the phase-shift error) is:

$$u_{err}(\delta,\alpha) = \frac{\lambda}{4\pi}\left(\arctan\frac{s_{ye}}{s_{xe}} - \arctan\frac{s_y}{s_x}\right) = \frac{\lambda}{4\pi}\left(\arctan\frac{\cos(\delta-\alpha)}{\cos\delta} - \arctan\frac{\sin\delta}{\cos\delta}\right) . \quad (12)$$

The phase-shift error region is bounded by the theoretical lines u_{errB} and u_{errb}. To calculate these boundaries we need to find the extremes of Eq. (12) with respect to δ. Those that give an error which is further away from the zero error are labeled δ_B, the others, which are closer to the zero error, are named δ_b. Substituting the locations of the extremes back into Eq. (12) gives the two bordering lines:

$$u_{errB}(\alpha) = u_{err}\left(\delta_B(\alpha),\alpha\right); \quad \text{where} \quad \delta_B(\alpha) = \frac{1}{2}\left(\alpha - \arccos\left(\frac{\sin\alpha - 1}{\cos\alpha}\right)\right) ,$$
$$u_{errb}(\alpha) = u_{err}\left(\delta_b(\alpha),\alpha\right); \quad \text{where} \quad \delta_b(\alpha) = \frac{1}{2}\left(\alpha + \arccos\left(\frac{\sin\alpha - 1}{\cos\alpha}\right)\right) . \quad (13)$$

Equations (13) represent a general theoretical result that depends only on the wavelength of the interferometric laser. It can also be applied to other quadrature-detection systems, such as optical encoders[9], where the constant $\lambda/(4\pi)$ in Eq. (12) is replaced by $p/(2\pi)$. Here, p is an arbitrary position period that equals $\lambda/2$ for the case of HQLI or λ/n for n-pass realizations of similar interferometers[10,11]. The results obtained with the HQLI can be therefore generalized to other quadrature-detection systems by replacing $\lambda/2$ with an arbitrary position period p.

4. RESULTS AND DISCUSSION

We used the HQLI to measure the displacement of the TM mounted on the PZT. The PZT was vibrating harmonically with frequency f = 70 Hz and amplitude A = 200 nm. The measurements were accomplished at various angles of the OWP rotation. The full revolution of 360° was realized in steps of 2°.

In order to compare the theoretical results presented in Vid. 1 with the experimental results, we show in Fig. 2 the measured photodiode signals V_x (the solid line) and V_y (the dashed line), when the phase shift deviates significantly from the ideal 90°. In Fig. 2(a) both signals are shown for the case, when there is no lack of quadrature. In this case, the measured visibilities are vis_x = 0.99 and vis_y = 0.97 (ideally they should be 1), and both signals have the same offsets and amplitudes. When the phase shift changes to α = −34° (Fig. 2(b)), the visibilities are: vis_x = 0.87 and vis_y = 0.95 (theoretically they should be: vis_x = 0.96 and vis_y = 0.98; see Vid. 1(b)). Additionally, the amplitudes and the offsets of both signals differ compared to Fig. 2(a), as can be seen in Fig. 2(b). Figure 2(c) shows the Lissajous curves for both cases. In the case of the ideal phase shift, the parametric curve (V_x,V_y) forms a circle. On the other hand, the lack of quadrature distorts this circle into an ellipse and moves its center due to different offsets of both signals.

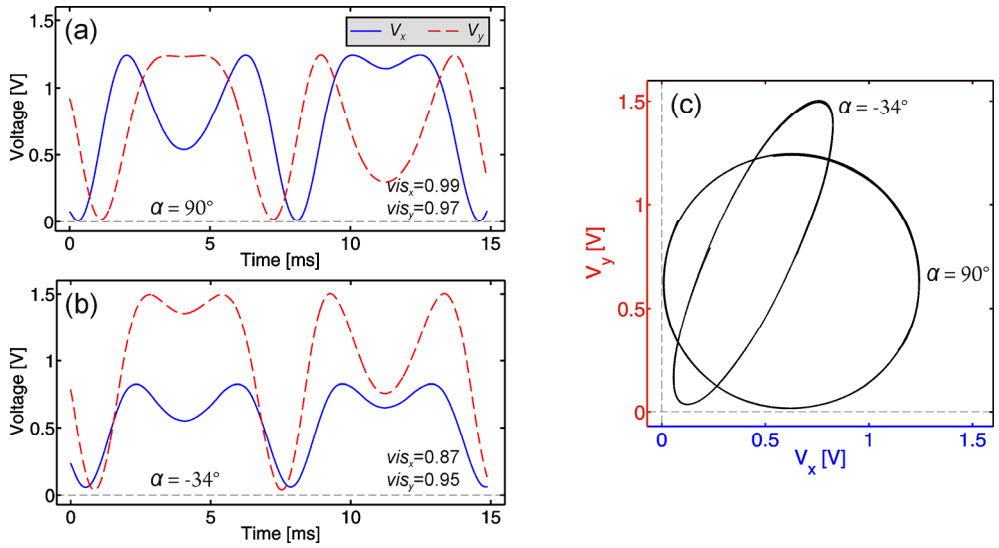

Figure 2. Comparison between the measured 2 kHz low-pass filtered photodiode signals obtained with: (a) an aligned interferometer and (b) an intentionally misaligned interferometer. (c) The parametric Lissajous representation of the measured signals. The circle is obtained from (a) and the ellipse from (b). The TM was mounted on a harmonically vibrating PZT with a frequency f = 70 Hz and an amplitude A = 200 nm.

In the ideal case, the dependence $\alpha(\varphi)$ is described by Eq. (6). Since the polarization-sensitive light reflections at certain optical elements may provide an additional constant phase shift, such as the reflection at the NBS, an extra constant term α_0 has to be added to the right-hand side of Eq. (6). To show and explain the origin of this extra phase shift, the measurements were carried out with two different beam splitters. A NBS was used in two series of measurements. In contrast to the first series, the NBS was rotated by 180° around the y-axis in the measurements of the second series. The third series was performed with a BS, which does not add an extra phase shift.

The three series of measurements of the $\alpha(\varphi)$ dependence for the two beam splitter settings are shown in Fig. 3(a). The phase shift α was extracted from each displacement measurement using the data processing algorithm described in Ref. 2. The measured phase shifts obtained with the NBS are depicted as circles. The top circles correspond to the measurements using a NBS, which adds an extra phase shift of 54°, while the bottom circles correspond to the

measurements performed with the same NBS rotated by 180° around the y-axis. In this case the sign of α_0 is changed. Here, the additional phase shift α_0 was measured by removing the OWP from the interferometer. In the case of the phase shift of the negative sign, the measured displacement has a wrong sign. To correct this, the signals V_x and V_y have to be exchanged. The measured data for the BS (with $\alpha_0 = 0$) are shown with squares in Fig. 3(a). The corresponding solid lines present the theoretical results given by Eq. (6) that were suitably shifted by adding the measured constant phase shift α_0. It has to be noted that the theoretical results were derived for the ideal octadic-wave plate. The lack of measured data in the interval ±10° results from the fact that the phase shift in this region can not be determined due to the extreme distortion of the Lissajous curve.

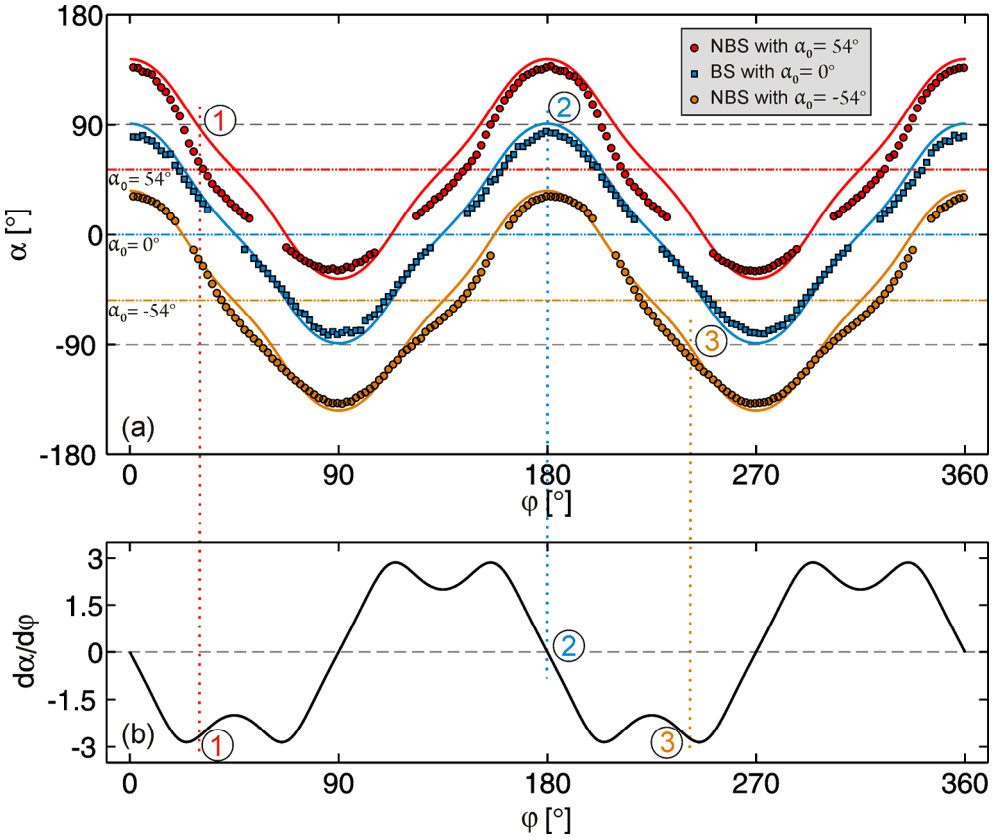

Figure 3. Dependence of the phase shift α on the OWP angle φ. (a) Solid lines are the theoretical curves (Eq. (6)) for the phase shift vs. OWP angle for different additional phase shifts α_0 originating from the (non-polarizing) beam splitter. The top points show the measurements of $\alpha(\varphi)$ for NBS with an additional phase shift $\alpha_0 = 54°$, the bottom points show the same dependence, when the same NBS was rotated by 180° around the y-axis. The middle points show measurement $\alpha(\varphi)$ for the beam splitter without an additional phase shift. (b) The theoretical sensitivity of the phase shift on the OWP rotation (Eq. (7)).

Figure 3(b) shows the theoretical sensitivity of the phase shift on the OWP rotation, which corresponds to the slope $d\alpha/d\varphi$ (Eq. (7)). A robust realization of an interferometer should minimize the influence of slight mechanical changes of optical components, such as the rotation of the OWP, on nonlinearities. In the HQLI, this can be achieved by using an ideal OWP with the nominal retardation value of $\lambda/8$, while the other optical components must not contribute any extra phase shift between the two polarizations. If this is true, the value $d\alpha/d\varphi = 0$ for an ideal 90°-phase shift, as can be seen from the dotted line (2) in Fig. 3. Therefore the phase shift in such an interferometer is insensitive on the OWP rotation.

On the other hand, when the constant value of the phase shift α_0 originates from the NBS (e.g, ±54° as in Fig. 3(a)), the OWP is used to add only the remaining phase shift, which is needed to attain the quadrature. As a consequence, such an interferometer is more sensitive to OWP rotation, as can be seen from the dotted lines (1) and (3) in Fig. 3. In the worst case, the rotation of 1° of the angle φ changes the phase shift for about 3°.

Figure 4 displays the measurements of $\alpha(\varphi)$ performed with the HQLI. Here the BS, which does not add any additional phase shift, was incorporated into the interferometer. The comparison between the measured data (squares) and the theoretical curve for the ideal OWP with the nominal retardation value of $\lambda/8$ (the solid line; Eq. (6)) reveals that the OWP, in our case, has a retardation value slightly smaller than $\lambda/8$. Due to this fact, the 90°-phase shift cannot be achieved. The dashed line in Fig. 4 shows a theoretical result obtained with a suitable wave plate retardation, which reaches a maximal phase shift of 82.5°.

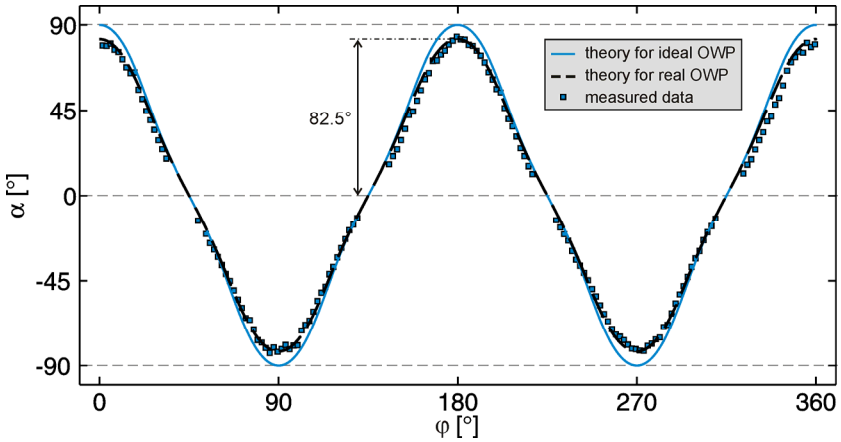

Figure 4. The solid line shows the theoretical dependence of the phase shift on the rotation of the ideal OWP (Eq. (7)). The dashed line shows the theoretical dependence for a real OWP. Points show measurements of this dependence for the beam splitter without an additional phase shift.

With a combination of the phase-shift-adding NBS and the OWP with retardation smaller than $\lambda/8$, the nonlinearities due to the lack of quadrature can be removed by a proper alignment of the OWP. However, this arrangement sets the interferometer in the region of its highest sensitivity on the rotation of the OWP. On the other hand, in the combination of the BS, without additional phase shift and the OWP with retardation smaller than $\lambda/8$, the quadrature cannot be achieved. Although the lack of quadrature can be determined and corrected by an appropriate signal processing, it always ruins the constant sensitivity due to which the resolution of the interferometer varies periodically. Moreover, an inappropriate phase shift also results in an unwanted reduction of the visibilities in both signals. Therefore the reduction of the phase-shift nonlinearity in quadrature-detection-based interferometers has a priority over the sensitiveness of crucial optical components on their mechanical changes, such as the rotation of the OWP.

Figure 5 shows results of the theoretical and experimental analysis of the displacement error originating from the lack of quadrature. Here we measured the displacement u_m of the TM at various values of α. This displacement was compared with the reference displacement u_r, measured with the aligned interferometer (at $\alpha = 0°$). The difference between the measured (the dashed line) and the reference (the solid line) displacement is shown in the bottom graphs of Figs. 5(a) and 5(b). The extremes of the error in Figs. 5(a) and 5(b) are shown as two circles in Fig. 5(d) at $\alpha = 140°$ (the error interval is indicated by "error 1") and at $\alpha = 45°$ (the error interval is indicated by "error 2"), separately. These two measurements were performed with the NBS with additional phase shift $\alpha_0 = 54°$. Equation (6) shows that the rotation of the OWP produces the phase shift α in the interval between −90° and 90°. However, in this case the NBS adds an additional phase shift $\alpha_0 = 54°$. Therefore the rotation of the OWP enables measurements of the phase shift in the interval between −36° and 144°.

When the NBS was rotated for the angle of 180° around the y-axis, the additional phase shift changed the sign, and was $\alpha_0 = -54°$. In this case the rotation of the OWP produces the phase shift in the interval between −144° and 36°. The measured and the reference displacement for the phase shift $\alpha = -35°$ are shown in the left-hand side of the Fig. 5(c). In this case it can be seen, that the measured (dashed line) displacement has the opposite sign in comparison with the reference displacement (solid line). Therefore, the signals V_x and V_y should be exchanged before the displacement error is calculated (see the right-hand side of Fig. 5(c)). The extremes of the error in Fig. 5(c) are shown as two circles in Fig. 5(d) at $\alpha = -35°$ and the error interval is indicated by "error 3".

In the case of the beam splitter without additional phase shift (squares in Fig. 5(d)), the rotation of the OWP produces the phase shift between the −82.5° and 82.5°, since we did not have an ideal OWP as was already described above. With both beam-splitters we can measure the phase shift in the interval between −140° and 140°. When the absolute value of the phase shift is smaller than 10° it can be no longer determined, because of the extreme distortion of the Lissajous curve. Therefore there is a lack of measured data in this interval.

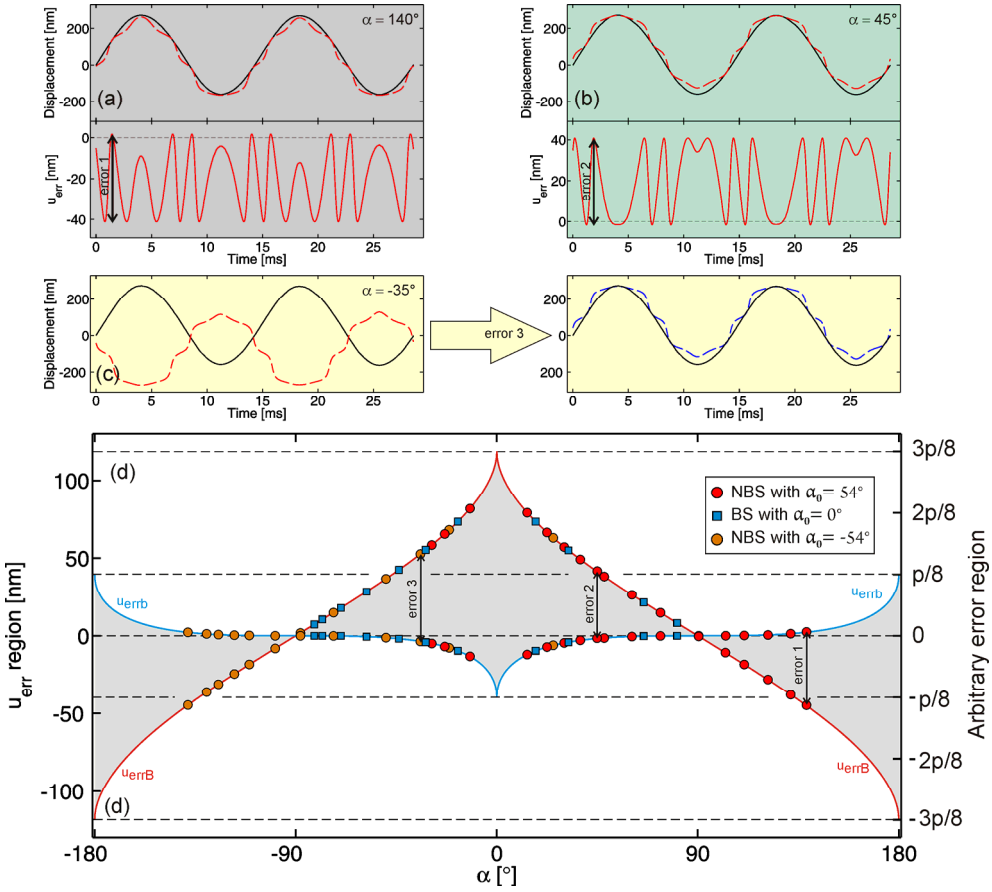

Figure 5. The influence of the phase shift on the displacement error. (a) The reference (α = 90°, solid line) and distorted (α = 43°, the dashed line) harmonic displacements and the corresponding error marked as "error 1". (b) The reference (α = 90°, the solid line) and distorted (α = 45°, the dashed line) displacements and the corresponding error marked as "error 2". (c) The reference and distorted (α = −35°) displacement. Before the phase-shift error is calculated, the signals V_x and V_y should be exchanged to obtain the correct direction of the displacement (right graph). (d) The phase-shift displacement error u_{err} as a function of the phase shift α for λ = 632.8 nm (left-hand scale) and the arbitrary position period p (right-hand scale). The measured border errors of the harmonic (f = 70 Hz, A = 200 nm) displacements measured with beam-splitters with different additional phase shifts for several values of α are marked as circles and squares. The solid lines show the theoretical error borders, calculated from Eqs. (13).

The shaded area in Fig. 5(d) displays the error region bounded by the theoretical lines (solid lines) u_{errb} and u_{errB} defined by Eqs. (13). The left-hand scale in Fig. 5(d) shows the error values for the period of the HQLI ($p = \lambda/2$; λ = 632.8 nm), while the right-hand scale shows the error for an arbitrary period p. At α = 0° the theoretical bordering line u_{errB} has a maximum value of $3p/8$, while u_{errb} has a minimum value of $-p/8$. At α = 180° these values change sign. When α = 0° the value $u_{errB} - u_{errb} = \lambda/4$ corresponds to the displacement of the TM, which causes the interference of the beams coming from the separate arms to change from constructive ($I_{x,y}^{\max}$) to destructive ($I_{x,y}^{\min}$).

5. CONCLUSION

We have presented the theoretical and experimental results showing the influence of the phase-shift error on the displacement measured by quadrature-based interferometers. This error was experimentally investigated using a homodyne quadrature laser interferometer, where the phase shift can be continuously varied by the rotation of the wave plate. We have shown that the rotation of the wave plate also produces unequal signal amplitudes, different zero offsets, and an unwanted reduction of the visibility in both signals. Moreover, the lack of quadrature ruins the constant sensitivity due to which the resolution of the interferometer varies periodically. It is, therefore, necessary to adjust the interferometer close to the optimal 90° phase shift.

For the robust realization of the interferometer based on the quadrature detection, any slight deviation of the optical components from the aligned position should not alter the nonlinearities. We have shown that this may pose a problem if an additional phase shift originates from the optical components in the interferometer.

The results presented in the displacement-error analysis have shown that the error region depends on the laser wavelength or, in general, on the position period of quadrature-detection systems. We have shown that this error is systematic, periodic and asymmetrical around the nominal displacement value. These results, obtained by the homodyne quadrature interferometer, can be applied to other quadrature-detection systems, even those which are not based on interferometry.

REFERENCES

[1] Požar, T., Gregorčič, P. and Možina, J., "Optical measurements of the laser-induced ultrasonic waves on moving objects," Optics Express 17(25), 22906-22911 (2009).

[2] Dai, G. L., Pohlenz, F., Danzebrink, H. U., Hasche, K. and Wilkening, G., "Improving the performance of interferometers in metrological scanning probe microscopes," Measurement Science & Technology 15(2), 444-450 (2004).

[3] Gregorčič, P., Požar, T. and Možina, J., "Quadrature phase-shift error analysis using a homodyne laser interferometer," Optics Express 17(18), 16322-16331 (2009).

[4] Bobroff, N., "Recent advances in displacement measuring interferometry," Measurement Science & Technology 4(9), 907-926 (1993).

[5] Bönsch, G. and Potulski, E., "Measurement of the refractive index of air and comparison with modified Edlén's formulae," Metrologia 35(2), 133-139 (1998).

[6] Ahn, J., Kim, J. A., Kang. C. S., Kim, J. W. and Kim, S., "A passive method to compensate nonlinearity in a homodyne interferometer," Optics Express 17(25), 23299-23308 (2009).

[7] Greco, V., Molesini, G. and Quercioli, F., "Accurate Polarization Interferometer," Review of Scientific Instruments 66(7), 3729-3734 (1995).

[8] Heydemann, P. L. M., "Determination and Correction of Quadrature Fringe Measurement Errors in Interferometers," Applied Optics 20(19), 3382-3384 (1981).

[9] Sanchez-Brea, L. M. and Morlanes, T., "Metrological errors in optical encoders," Measurement Science & Technology 19(11), 115104 (2008).

[10] Usuda, T. and Kurosawa, T., "Calibration methods for vibration transducers and their uncertainties," Metrologia 36(4), 375-383 (1999).

[11] Pisani, M., "Multiple reflection Michelson interferometer with picometer resolution," Optics Express 16(26), 21558-21563 (2008).